

## RESEARCH ARTICLE

# Carbene-Catalyzed Phthalide Ether Functionalization for Discovering Chiral Phytovirucide that Specifically Targets Viral Nia Protein to Inhibit Proliferation

Xiaoyi Wang<sup>1</sup>, Weijia Yang<sup>1</sup>, Shang Wu<sup>1</sup>, Fangru Jin<sup>1</sup>, Zhongjie Shen<sup>1</sup>, Xiangyang Li<sup>1\*</sup>, Yonggui Robin Chi<sup>1,2</sup>, Baoan Song<sup>1</sup>, and Runjiang Song<sup>1\*</sup>

<sup>1</sup>State Key Laboratory of Green Pesticide, Center for R&D of Fine Chemicals of Guizhou University, Guiyang 550025, P. R. China. <sup>2</sup>School of Chemistry, Chemical Engineering, and Biotechnology, Nanyang Technological University, Singapore 637371, Singapore.

\*Address correspondence to: [songrj@gzu.edu.cn](mailto:songrj@gzu.edu.cn) (R.S.); [xyli1@gzu.edu.cn](mailto:xyli1@gzu.edu.cn) (X.L.)

Plant diseases caused by vegetable viruses are an important threat to global food security, presenting a major challenge for the development of antiviral agrochemicals. Functional proteins of plant viruses play a crucial role in the viral life cycle, and targeted inhibition of these proteins has emerged as a promising strategy. However, the current discovery of antiviral small molecules is hampered by the limitations of synthetic approaches and the narrow range of targets. Herein, we report a practical application of organocatalysis for serving pesticide discovery that bears a unique molecular basis. An *N*-heterocyclic carbene-modulated reaction is first designed to asymmetrically functionalize diverse natural phenols with phthalides. Our designed method is capable of producing a series of new phthalidyl ethers under mild conditions with good yields, enantioselectivity, and functional group tolerance. Among these, compound (*R*)-**3w** exhibits excellent and enantioselectivity-preferred curative activity against potato virus Y (PVY). Mechanistically, it is proposed that (*R*)-**3w** interacts with the nuclear inclusion body A (Nia) protein of PVY at the His150 residue. This binding impairs Nia's function to cleavage polyprotein, thereby inhibiting formation of viral replication complex. The study provides insights into advancing synthetic protocol to facilitate agrochemical discovery, and our identified (*R*)-**3w** may serve as a potential lead for future research and development PVY-Nia inhibitors.

## Introduction

Currently, the global population continues to grow, with projections indicating that by 2050, there will be nearly 10 billion people requiring sustenance [1–4]. In addition, the unpredictability of weather patterns can lead to crop failures, reduced agricultural land productivity, and increased vulnerability to pests and diseases [5–7]. The intricate tapestry of global food security is increasingly being strained by the dual challenges of climate change and a burgeoning population. In the face of these issues, ensuring food security while adhering to the principles of sustainable development is a formidable task, which necessitates the urgent development of sustainable plant protection strategies [8,9]. “Green” pesticides are characterized not only by their high efficacy in pest control and management, but also by their safety for nontarget organisms and humans. Meanwhile, the process of preparing these pesticides must adhere to principles of sustainability [10–12]. Asymmetric catalysis has emerged as a potent tool for discovering or manufacturing useful molecules with stereoselectivity-driven bioactivities, such as asymmetric hydrogenation to Ramipril and Montelukast [13,14].

Within this field, asymmetric synthesis enabled by organocatalysis, owing to its advantages of simple operation, mild conditions, metal-free nature, and relative sustainability, holds promise for the development of green agrochemicals [15–17]. Despite the success of organocatalysis in pharmaceutical synthesis and polymer preparation and degradation, its application in pesticide discovery is still limited [18–22].

Potato virus Y (PVY) is a significant plant pathogen belonging to the *Potyvirus* genus within the family *Potyviridae*. It is widely recognized as one of the most economically detrimental viruses affecting potato crops (*Solanum tuberosum*) and other solanaceous plants, including peppers and tomatoes [23–27]. PVY management has remained a pending problem in agricultural chemistry, stemming from the evolutionary resistance of its vector insect, the aphid, to insecticides, as well as the repetitive molecular targets of existing antiviral agents [28–30]. Based on the genome of PVY, it encodes a total of 10 functional proteins, including the coat protein (CP), nuclear inclusion body A (Nia) protein, the first protein, helper component-proteinase, etc. [31]. These proteins play crucial roles in the PVY life cycle, pathogenic behavior, and virulence. Interfering

**Citation:** Wang X, Yang W, Wu S, Jin F, Shen Z, Li X, Chi YR, Song B, Song R. Carbene-Catalyzed Phthalide Ether Functionalization for Discovering Chiral Phytovirucide that Specifically Targets Viral Nia Protein to Inhibit Proliferation. *Research* 2025;8:Article 0637. <https://doi.org/10.34133/research.0637>

Submitted 28 December 2024

Revised 17 February 2025

Accepted 21 February 2025

Published 14 March 2025

Copyright © 2025 Xiaoyi Wang et al. Exclusive licensee Science and Technology Review Publishing House. No claim to original U.S. Government Works. Distributed under a Creative Commons Attribution License (CC BY 4.0).

with these key viral proteins using small molecules has emerged as a promising antiviral strategy. Indeed, a number of potential small molecules focusing on PVY CP have been progressively uncovered [32–34]. For instance, our previous work on *N*-heterocyclic carbene (NHC)-mediated [3+4] cycloaddition discovered a chiral antiviral compound with a unique molecular structure of arylimidazole-fused diazepine and mechanism that competitively inhibits the interaction between CP and plant host factor, thereby disabling the virion's ability to move across cells [35]. Additionally, the commercially available drug ningnanmycin has been suggested to exert its antiviral effects by binding to CP [33,36]. However, though CP is important for protecting the PVY genome and facilitating intercellular traffic, antivirals with a similar mechanism of action are susceptible to

resistance induced by point mutations [37–39]. Therefore, it is worthwhile to investigate potential small molecules beyond serving inhibitors of CP. Unfortunately, to our knowledge, compounds targeting other functional proteins of PVY have yet to be identified.

In our pursuit to identify new molecules with potential anti-PVY activity, phthalides have garnered significant attention. These derivatives possess a wide range of biological properties and have been explored for treating ischemic stroke and acute coughing, as well as for their antifungal and herbicidal applications (Fig. 1A) [40–42]. Furthermore, phthalide esters are commonly employed as prodrug moieties in pharmaceutical design. In contrast, there is a paucity of studies concerning their antiviral properties. Jia et al. [43] were the first to isolate a unique

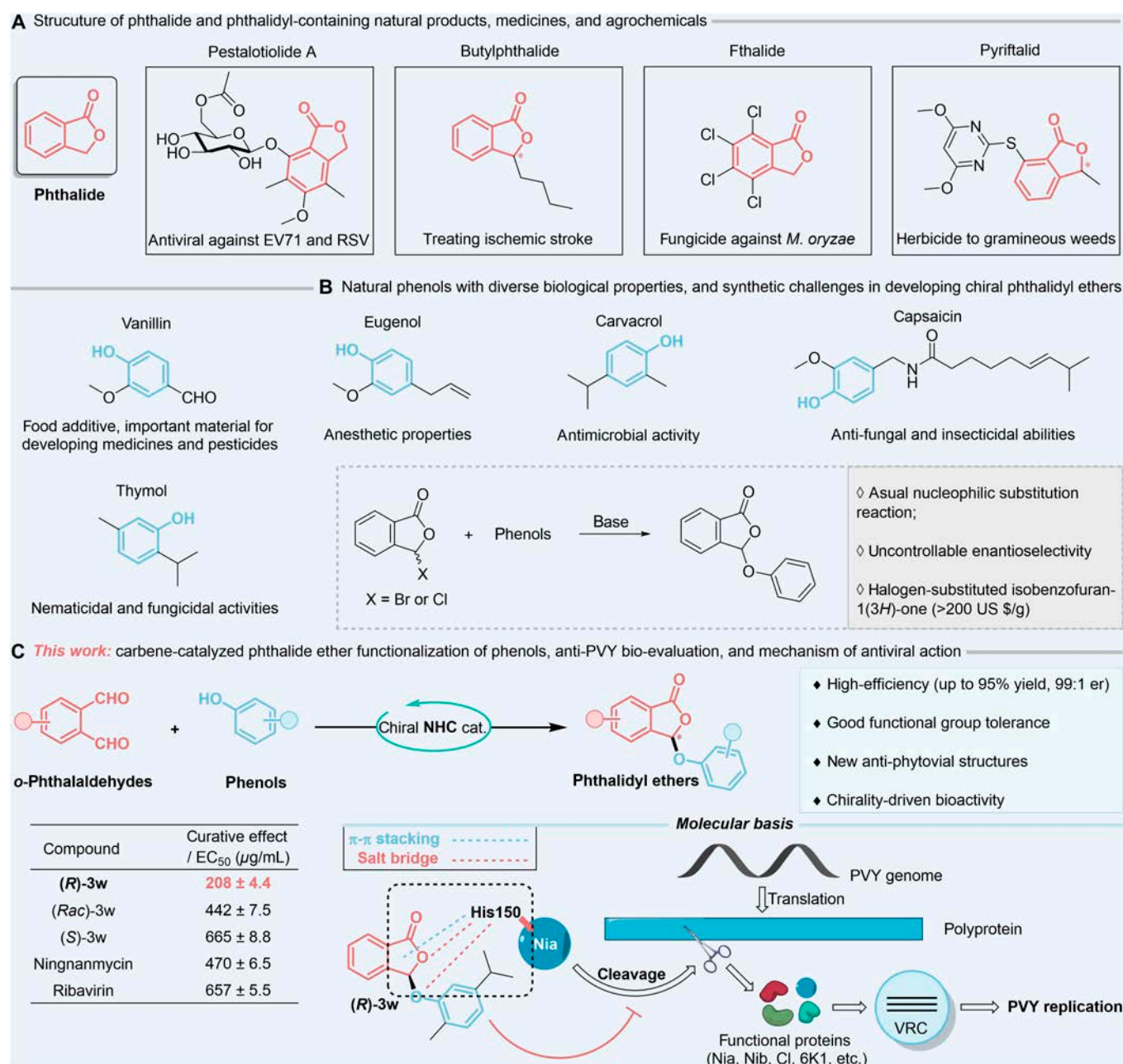


**Fig. 1.** Discovery of phthalide antivirals with unique mechanisms of action. (A) Structure of phthalide and phthalidyl-containing natural products, medicines, and agrochemicals. (B) Natural phenols with diverse biological properties and synthetic challenges in developing chiral phthalidyl ethers. (C) Carbene-catalyzed phthalide ether functionalization of phenols, anti-PVY bio-evaluation, and mechanism of antiviral action.

phthalidyl ether, pestalotioid A, from the fermentation broth of *Pestalotiopsis* sp., which exhibited an inhibitory impact against enterovirus 71 and respiratory syncytial virus. This indicates that phthalide ethers may constitute promising leads for developing phytovirucides with innovative mechanisms of action. Furthermore, many natural phenols possess diverse structures and pesticidal activities and are available at a low market price. In terms of antimicrobial properties, thymol has already been registered as a pesticide [44–46]. Consequently, natural phenols can serve as promising fragments for the construction of ether bonds with phthalides. The 3-position of phthalides is the primary site for derivatization, yet challenges persist, especially in the asymmetric introduction of active groups at this site, which could enhance the specific binding of molecules to targets and reduce the risk to nontarget organisms. Conventional methods involve the substitution reaction of phenols with 3-halogenoisobenzofuran-1(3*H*)-one that is constrained in the discovery of pesticides due to the inability to control enantioselectivity and the high cost of initial materials (Fig. 1B).

Herein, we report a carbene-catalyzed phthalide ether functionalization of phenol compounds, facilitating facile synthesis of a variety of optically enriched aryl phthalidyl ethers (Fig. 1C). A myriad of differently substituted phenols, even natural phenols, can be converted into their corresponding products with outstanding enantioselectivity (up to 99:1 er) and conversion rates (up to 95% yield) under our optimal condition catalyzed by NHC. We further discovered that the phthalide ether derivative (*R*)-**3w** of carvacrol possesses potent activity against PVY through bio-evaluations. Specifically, it displayed

substantially superior and enantioselectivity-preferred curative effects in comparison to the popular commercial drugs ningnanmycin and ribavirin, as well as its enantiomer (*S*)-**3w** and racemic mixture (*Rac*)-**3w**, which encouraged subsequent mechanism of action investigations. It is noteworthy that the curative effect of a drug usually correlates with its impact on pathogen replications, and the current mechanisms of antiviral action in plants are primarily based on the protective and inactivating activities of virucides [47]. Combining molecular docking with a series of molecular biological validations allows one to reasonably hypothesize that (*R*)-**3w** may act on a brand-new molecular target via His150 residue, namely, the Nia involved in cleavage of the viral polyprotein into functional proteins. Several of these proteins are essential for generation of the viral replication complex (VRC), which mediates PVY replication. Both the mutation at site 150 and (*R*)-**3w** treatment significantly reduced the proliferation of PVY in *Nicotiana benthamiana* (*N. benthamiana*). We expect this study to contribute novel antiviral structures, asymmetric synthetic protocol, and potential new target protein for the PVY management.

## Results and Discussion

### Synthetic methodology

Our initial attempt involved the use of phenol (**1a**) and aldehyde (**2a**) as standard substrates under the catalysis of NHC precursor **A** [48] and the mediation of oxidant quinone (DQ). These starting materials are commercially available and inexpensive. The primary results obtained are presented in Fig. 2.

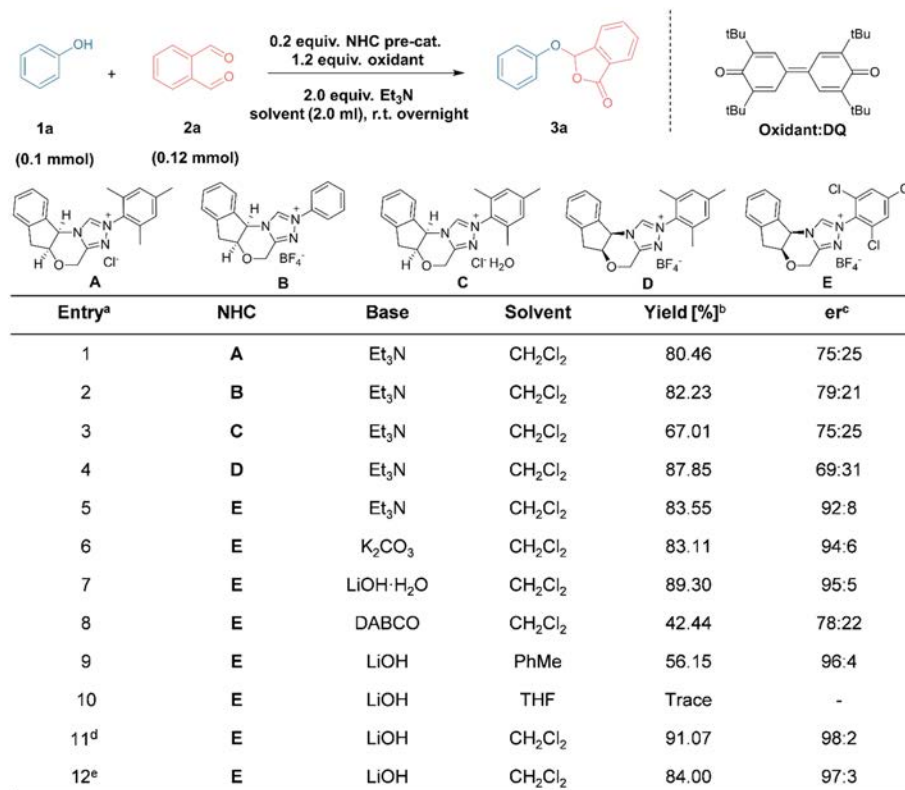


**Fig. 2.** Optimization of reaction conditions <sup>a</sup> Unless otherwise specified, the reactions were carried out with **1a** (0.1 mmol), **2a** (0.12 mmol), NHC (20 mol%), base (200 mol%), DQ (120 mol%), CH<sub>2</sub>Cl<sub>2</sub> (2 ml), 12 h, r.t. <sup>b</sup> Isolated yield. <sup>c</sup> Determined by chiral HPLC analysis (IB column, 0.6 ml/min, hexane/*i*PrOH = 80/20). <sup>d</sup> Determined by chiral HPLC analysis (IB column, 0.6 ml/min, hexane/*i*PrOH = 80/20); **1a** (0.1 mmol), **2a** (0.12 mmol), NHC (20 mol%), DQ (120 mol%), base (200 mol%), 4Å MS (80 mg), solvent (2 ml), 12 h, r.t. <sup>e</sup> **1a** (0.1 mmol), **2a** (0.12 mmol), NHC (20 mol%), DQ (120 mol%), base (200 mol%), solvent (2 ml), 12 h, 0 °C.

Encouragingly, a decent yield was achieved, and the title product **3a** was observed to be nonracemic (Fig. 2, entry 1). Under the same conditions, modifying the *N*-mesityl group of the catalyst to an unsubstituted phenyl group (to produce catalyst **B** [49]) slightly enhanced both the yield and the optical purity of the product (entry 2). In contrast, the use of the hydrated form of **A**, namely, catalyst **C** [50], led to a decrease in yield (entry 3). Considering that the different anion might also influence reactivity [51], we replaced pre-catalyst **A** with its tetrafluoroborate form **D** [52], but it did not yield satisfactory results (entry 4). Based on previous studies suggesting the reversible addition of the NHC to aldehydes regulated by the *N*-substituent of the catalyst, which affects the formation of the Breslow intermediate [53], we further introduced electron-withdrawing groups into the *N*-aryl ring. With the assistance of triazole salt **E** [54], the conversion of the reaction could be maintained above 80% while significantly enhancing the enantioselectivity (entry 5). Moreover, the reaction could proceed with either organic or inorganic bases, but the latter generally provided better stereoselectivity in this case (entries 6 to 8). The choice of solvent had a pronounced impact on the reaction, with solvents other than dichloromethane yielding adverse effects on the reaction outcomes (entries 9 to 11). Additionally, conducting the reaction at lower temperatures, such as 0 °C, did not further enhance the optical purity of the product while also reducing the yield (entry 12). Overall, we favor the combination of entry 11 as the optimal condition for the reaction (for the detailed optimization process, please refer to Table S1).

Armed with the optimized reaction conditions, we next explored the scope of the reaction using various phenols **1** and substituted *o*-phthalaldehydes **2**. As shown in Fig. 3A, the reaction tolerated phenols with electron-withdrawing and electron-donating groups, as well as multiply substituted species, affording relatively high yields and enantiomeric ratios (**3b** to **3r**). Bioisosteric replacement is a widely used strategy in drug design; therefore, we attempted to change phenol with its bioisosteres thiophenol upon the same condition. The reaction proceeded successfully with thiophenol, producing the corresponding product in good yield with slightly reduced enantioselectivity (**3p**). Furthermore, the use of substituted *o*-phthalaldehydes also led to the corresponding derivatives without a significant decrease in *er* values. Notably, phenolic structures are common in natural products, pesticides, and pharmaceuticals, exhibiting a broad range of biological activities [55–57]. For example, fenhexamid, a commercialized fungicide developed by Bayer, is primarily used to control plant diseases such as gray mold, sclerotinia, and black spot [58]. Thymol, another phenolic compound, is registered as an active component in pesticide products utilized as an animal repellent, microbicide, disinfectant, and anti-tubercular agent [44,45]. To our delight, these structurally unique phenolic ingredients demonstrated good functional group tolerance in the reaction, providing phthalide-functionalized products with high optical purity (Fig. 3A, **3s** to **3z**). This phthalide ether functionalization reaction was preliminary assessed at the gram scale using **3w** as an example (Fig. 3B). Upon increasing the reaction conditions, including the quantities of substrate, catalyst, and oxidant, by a factor of 100, the conversion rate enhanced while the enantioselectivity remained consistent.

To elucidate the mechanistic underpinnings of our synthetic methodology, we proposed a preliminary catalytic cycle as depicted in Fig. 4. The inferred reaction pathway involves the

following sequence: The NHC precatalyst undergoes deprotonation under basic conditions to generate a catalytically active free NHC species. This species subsequently reacts with phthalaldehydes **2** in the presence of an oxidant, forming NHC-bound intermediates **I** [59]. Intermediates **I** then engage with phenolic substrates **1** via nucleophilic attack at the carbonyl group, yielding **2** stereochemically distinct intermediates (**II** and **III**), contingent upon the trajectory of nucleophilic addition (upper or lower face of the carbonyl moiety). Although this step is theoretically reversible, the steric bias imparted by the chiral NHC framework enforces a kinetic preference for the formation of intermediates **III**. Subsequent addition–elimination steps generate intermediates **IV**, which releases the free NHC to reinitiate the catalytic cycle while affording the target products **3**. Recently, carbene-mediated reactions have emerged as a powerful tool for stereoselective optimization of hydroxyl-containing bioactive constituents (e.g., saccharides, carboxylic acids, aldehydes, and alcohols) in drugs and natural products, yet their application in phenolic compound modification remains underexplored [60–64]. Beyond advancing synthetic methodologies, the characterization of novel types of chirality may facilitate the discovery of functional molecules with exciting properties [65–68]. To sum up, our synthetic protocol can efficiently achieve functionalization and modification of complex phenols with different substituting patterns or even natural ones with good stereoselectivity and scalability, which is expected to serve the discovery of medicines or pesticides.

### Anti-PVY evaluations

PVY-induced viral diseases have a detrimental impact on the sustainable yield of solanaceous crops. Current antiviral strategies mainly focus on managing the vector aphids, using specific insecticides such as pymetrozine or neonicotinoids [69]. However, the repertoire of direct antiviral agents remains relatively limited. Many phenolic and phthalide derivatives are known to possess significant antimicrobial potential [44–46,55–58]. To thoroughly evaluate the practical utility of our developed synthetic method in plant protection, we systematically assessed the antiviral activity of all synthesized products against PVY (Tables 1 and 2), using commercially available antiviral agents ningnanmycin and ribavirin as positive controls. Several of our synthesized isobenzofuran-1(3*H*)-one derivatives exhibited promising antiviral activity, with compound (*R*)-**3w** demonstrating superior curative efficacy compared to 2 commercial antivirals. We also tested the anti-PVY activity of carvacrol, which demonstrated limited efficacy. This observation precludes the possibility of intrinsic antiviral activity in carvacrol itself and confirms that structural modification with phthalide significantly enhances its bioactivity against PVY. Preliminary structure–activity relationship analysis based on anti-PVY activity indicated that most chiral isobenzofuranone derivatives synthesized from phenolic compounds with natural bioactivity exhibited moderate to excellent protective, curative, and inactive effect against PVY (e.g., **3s**, **3v**, **3w**, and **3y**). Compared with the commercial reference drugs ningnanmycin and ribavirin, compound **3v** derived from the thymol isomer of carvacrol exhibited appreciable antiviral activity against PVY, although its efficacy was lower than that of compound (*R*)-**3w**, which also demonstrated excellent curative activity against PVY. This suggests that the steric hindrance of the substituents may be a critical factor influencing antiviral activity. Compounds **3b**, **3c**, and **3d**, with identical

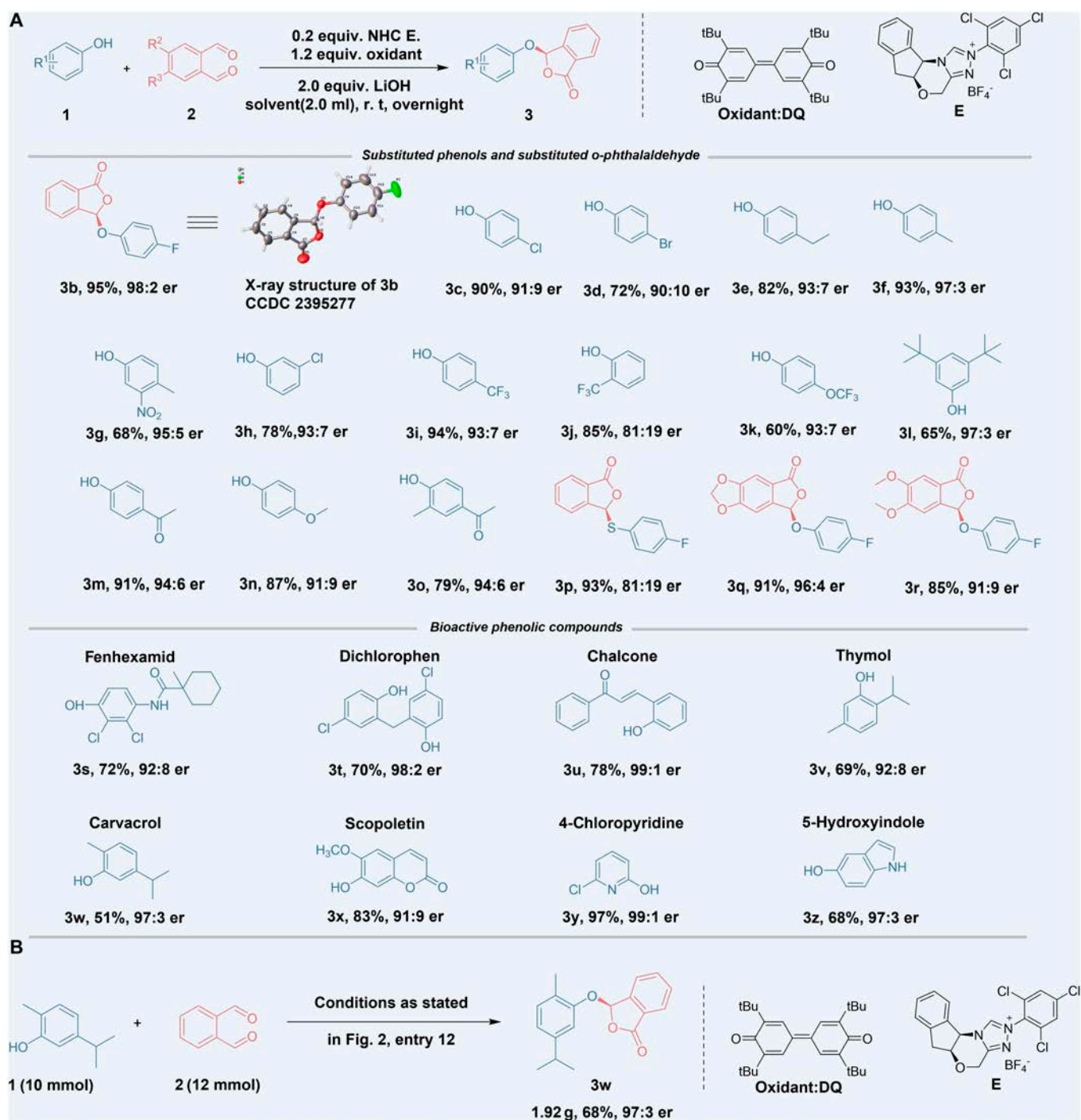


**Fig. 3.** (A) Reaction scope of phenolic compound **1** and ortho benzaldehyde substrate **2**. The reaction conditions are shown in Fig. 2, entry 12. The yield is the isolated yield after purification by column chromatography. The Er value is determined by HPLC on a chiral stationary phase. (B) Gram-scale preparation of (*R*)-**3w** using our developed catalysis.

electron-withdrawing groups (such as -F, -Cl, and -Br), exhibited similar curative, protective, and inactivating activities against PVY. Substituting phenol with thiophenol (e.g., **3p**) enhanced the inactivating activity against PVY. Additionally, compounds **3q** and **3r** further illustrated the significant impact of the steric hindrance of substituents on the antiviral activity.

Chiral pesticides have emerged as potent tools for achieving selective control of agricultural pests. Enantiomers within a pair can display significantly different performances in pest control, toxicity to nontarget organisms, and even distinct fates

in the environment [70,71]. A representative instance is metolachlor, a widely used herbicide effective against grass and broadleaf weeds. However, *S*-metolachlor has been demonstrated to possess better herbicidal activity and bio-safety compared to its *R*-enantiomer [72,73]. On this basis, we selected the (*R*)-**3w** identified in our previous bio-screening for further investigation. With assistance from the enantiomer of pre-catalyst **E** and an achiral NHC catalyst, we successfully synthesized the *S*-enantiomer [(*S*)-**3w**] and the racemic mixture (*Rac*)-**3w** of (*R*)-**3w**. By further comparing their protective

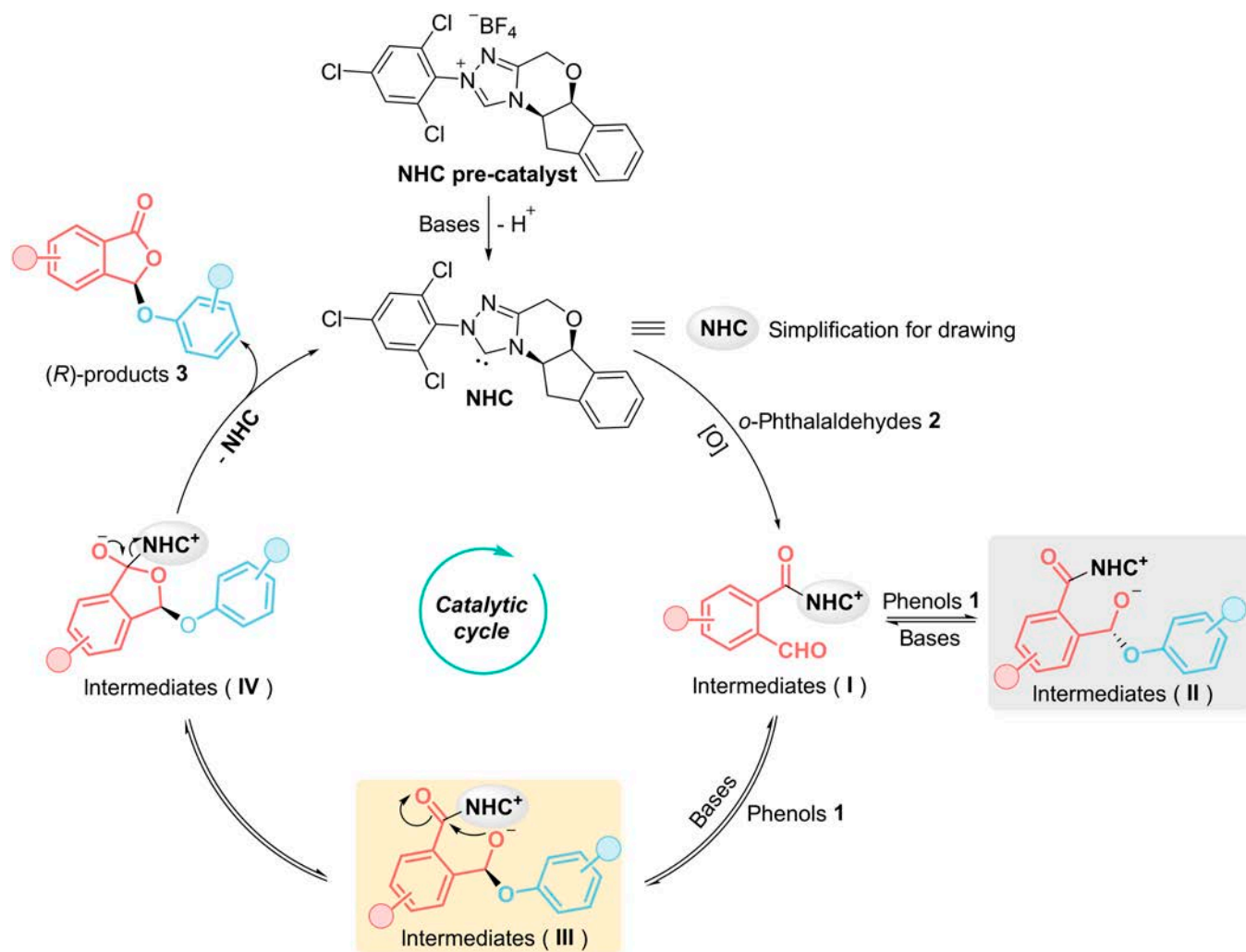


Fig. 4. Speculated mechanism of our developed NHC-catalyzed phthalide ether functionalization of phenols.

activities against PVY, we were surprised to find that the *R* isomer had a significantly lower  $\text{EC}_{50}$  value than its enantiomer and racemate. The results of the biological evaluation provide more evidence that supports the great potential of our synthetic approach in pesticide discovery. Compound (*R*)-**3w** with a novel structure may behave as an efficient chiral phytoviricide, and it is worth exploring whether it has a unique mechanism of action.

### Mechanism of antiphytoviral action

Currently, there are 2 main explanations for the mechanisms of action of antiviral agrochemicals. The first is drugs serving as plant immune inducers in preventing and controlling viral infections by activating the plant's innate immune responses [74]. These inducers trigger the production of signaling molecules such as salicylic acid, jasmonic acid, and ethylene [75]. Upon activation, these signaling molecules induce the expression of defense-related genes, including those encoding pathogenesis-related (PR) proteins, which have antiviral properties [76]. PR proteins can directly interfere with viral replication and movement within the plant, as well as enhance the plant's structural and biochemical defenses. Additionally, immune inducers can activate systemic acquired resistance, a long-lasting and broad-spectrum resistance mechanism that primes

the plant to more effectively defend against future viral attacks [75]. In most cases, these pesticides exhibit favorable protective activity. Another straightforward basis is inactivation of viral replication, motility and infection, which can be realized through molecules that target the viral RNA or proteins [77–80]. Recently, numerous examples of using small-molecule inhibitors to inactivate the PVY CP have emerged, and despite sharing the same target, their mechanisms of action are not identical [81–83]. For instance, benzo[*b*]thiophene and 2*H*-chromene-based analogues may interfere with viral particle formation by competing for the binding sites of CP to nucleic acids [84], whereas arylimidazole-fused diazepines have been reported to disrupt the interaction between CP and host pro-viral factors, thereby affecting the intercellular movement of viral particles [85]. These studies are often based on the superior inactivation activity of small molecules. In contrast, our compound has shown curative effects in tests with infected plants. Typically, during the early stages of infection, the drug may achieve its purpose by interfering with the efficient proliferation of the virus. PVY proliferation depends on the proper execution of genomic replication functions, which requires the coordinated regulation of several functional proteins. Among them, Nia acts as a critical scissor, responsible for cleaving the polyprotein translated from the genome into essential functional proteins

**Table 1.** Anti-PVY activities of the compounds **3b-3z**(*R*) (500 µg/ml)

Compound <sup>a</sup>	Curative effect (%)	Protective effect (%)	Inactive effect (%)
3b	52.37 ± 0.61	42.69 ± 3.50	52.28 ± 3.52
3c	54.95 ± 3.27	45.17 ± 2.52	51.28 ± 3.88
3d	38.58 ± 4.10	39.21 ± 1.36	42.56 ± 0.89
3e	30.82 ± 4.65	43.73 ± 4.28	40.08 ± 1.71
3f	49.82 ± 4.78	52.90 ± 4.48	49.75 ± 1.31
3g	58.00 ± 4.46	31.22 ± 3.47	52.26 ± 0.76
3h	36.88 ± 2.86	32.52 ± 2.44	55.04 ± 4.92
3i	43.67 ± 3.44	59.82 ± 3.04	52.83 ± 3.61
3j	43.65 ± 4.66	51.17 ± 2.49	45.10 ± 3.58
3k	47.53 ± 7.79	37.68 ± 3.73	55.84 ± 1.86
3l	30.63 ± 4.99	31.15 ± 4.13	47.13 ± 3.58
3m	40.49 ± 2.13	57.46 ± 0.85	40.28 ± 3.65
3n	42.45 ± 3.50	46.02 ± 3.30	38.82 ± 1.43
3o	39.61 ± 1.29	44.54 ± 3.15	39.12 ± 1.11
3p	31.00 ± 4.52	42.15 ± 3.37	63.50 ± 3.46
3q	54.88 ± 4.54	55.57 ± 2.60	52.64 ± 1.81
3r	50.44 ± 1.32	54.45 ± 3.47	51.66 ± 4.28
3s	34.90 ± 2.49	34.05 ± 3.50	57.23 ± 4.55
3t	33.87 ± 2.23	47.47 ± 2.62	41.88 ± 0.86
3u	46.29 ± 1.91	47.45 ± 2.57	40.33 ± 1.95
3v	54.26 ± 0.61	45.52 ± 2.60	55.45 ± 4.96
3w	67.30 ± 1.30	46.95 ± 4.46	61.16 ± 3.99
3x	37.37 ± 4.84	48.68 ± 2.59	44.23 ± 2.07
3y	30.90 ± 3.98	30.90 ± 3.98	52.76 ± 2.15
3z	40.20 ± 4.48	47.77 ± 3.17	40.20 ± 4.48
Carvacrol	31.81 ± 1.41	36.00 ± 2.80	44.15 ± 0.72
NNM <sup>b</sup>	50.69 ± 3.38	51.6 ± 3.02	85.9 ± 2.34
RBV <sup>c</sup>	45.04 ± 3.61	51.5 ± 4.89	62.6 ± 2.22

<sup>a</sup>All data were average data of 3 replicates. Ribavirin was used as the positive control.

<sup>b</sup>NNM, ningnanmycin.

<sup>c</sup>RBV, ribavirin.

necessary for subsequent self-reproduction [86,87]. Therefore, we propose that Nia might be the primary target of (*R*)-**3w** and aim to verify this hypothesis.

The identification of crystal structures of molecular targets in pest organisms contributes to the opportunity for specific design of new pesticides [88]. So far, among the protein components of PVY, only the structural basis of CP and VPg has been elucidated [90]. To determine the binding sites of small molecules on Nia, we performed homology modeling with the reported sequence to construct a 3-dimensional (3D) structural model of PVY-Nia (Fig. 5A). In the Ramachandran plot analysis, it is evident that 94.55% (Fig. 5B and supporting data are presented in Fig. S1) of the amino acid residues are located within the favored regions, indicating that the constructed

**Table 2.** EC<sub>50</sub> values of the (*R*)-**3w**, (*Rac*)-**3w**, and (*S*)-**3w** anti-PVY in vivo (µg/ml)

Compound <sup>a</sup>	Curative effect (%)	Curative effect (EC <sub>50</sub> )
( <i>R</i> )- <b>3w</b>	67.30 ± 1.30	208 ± 4.4
( <i>Rac</i> )- <b>3w</b>	50.35 ± 3.51	442 ± 7.5
( <i>S</i> )- <b>3w</b>	40.57 ± 3.18	665 ± 8.8
NNM <sup>b</sup>	50.69 ± 3.38	470 ± 6.5
RBV <sup>c</sup>	45.04 ± 3.61	657 ± 5.5

<sup>a</sup>All data were average data of 3 replicates. ribavirin was used as the positive control.

<sup>b</sup>NNM, ningnanmycin.

<sup>c</sup>RBV, ribavirin.

model is of satisfactory quality and can be utilized for further structural and functional studies. The molecular docking results (Fig. 5C and D) demonstrate that (*R*)-**3w** formed multiple interactions with PVY-Nia, including  $\pi$ -cation and  $\pi$ -alkyl interactions with H150, along with salt bridges. Additionally, I124 engaged in  $\pi$ - $\sigma$  interactions with the compound. Quantitative analysis revealed bond lengths of 3.6 Å for the H150  $\pi$ -cation interaction and 3.9 Å for the I124  $\pi$ - $\sigma$  interaction. Given that shorter bond lengths correlate with lower energy states (indicating enhanced system stability) and considering interaction multiplicity preferences [91–93], we prioritized H150 for mutagenesis. The calculated binding energy between (*R*)-**3w** and wild-type Nia protein was  $-5.884$  kcal/mol. Subsequent mutations at I124 and H150 residues yielded binding energies of  $-5.853$  and  $-5.158$  kcal/mol, respectively. The substantial energy shift following H150 mutation indicates its critical role in maintaining binding stability. Notably, the less active (*S*)-**3w** enantiomer docking revealed no H150 interactions, confirming residue specificity. To thoroughly assess the binding stability of the compound (*R*)-**3w** with the receptor protein, we conducted molecular dynamics simulations. The conformational stability, represented by the changes in root-mean-square deviation over the simulation time, is illustrated in Fig. 5E. Through this simulation approach, we were able to observe and quantify in detail the stability of the binding between the compound (*R*)-**3w** and the receptor protein. Moreover, after (*R*)-**3w** binds to protein, the value becomes smaller. The overall stability is more stable. The analysis revealed that the (*R*)-**3w** PVY Nia complex attained stability after 15 ns, indicating that the system had reached an equilibrium state (Fig. 5E). Furthermore, the binding free energy of the compound (*R*)-**3w** to the PVY Nia molecular dynamics trajectory was calculated using the molecular mechanics Poisson–Boltzmann surface area method, yielding a value of  $-42.37$  kcal mol<sup>-1</sup>. These preliminary experimental findings corroborate our hypothesis that the compound (*R*)-**3w** binds to Nia through  $\pi$ -cation interactions,  $\pi$ -alkyl interactions, and salt bridges and have identified a potential binding site (H150). These findings are consistent with the results of previous activity assays and support the hypothesis that the chirality-driven activity differences between the enantiomers are possibly attributed to their binding affinities to the potential target. In addition, the superior interaction

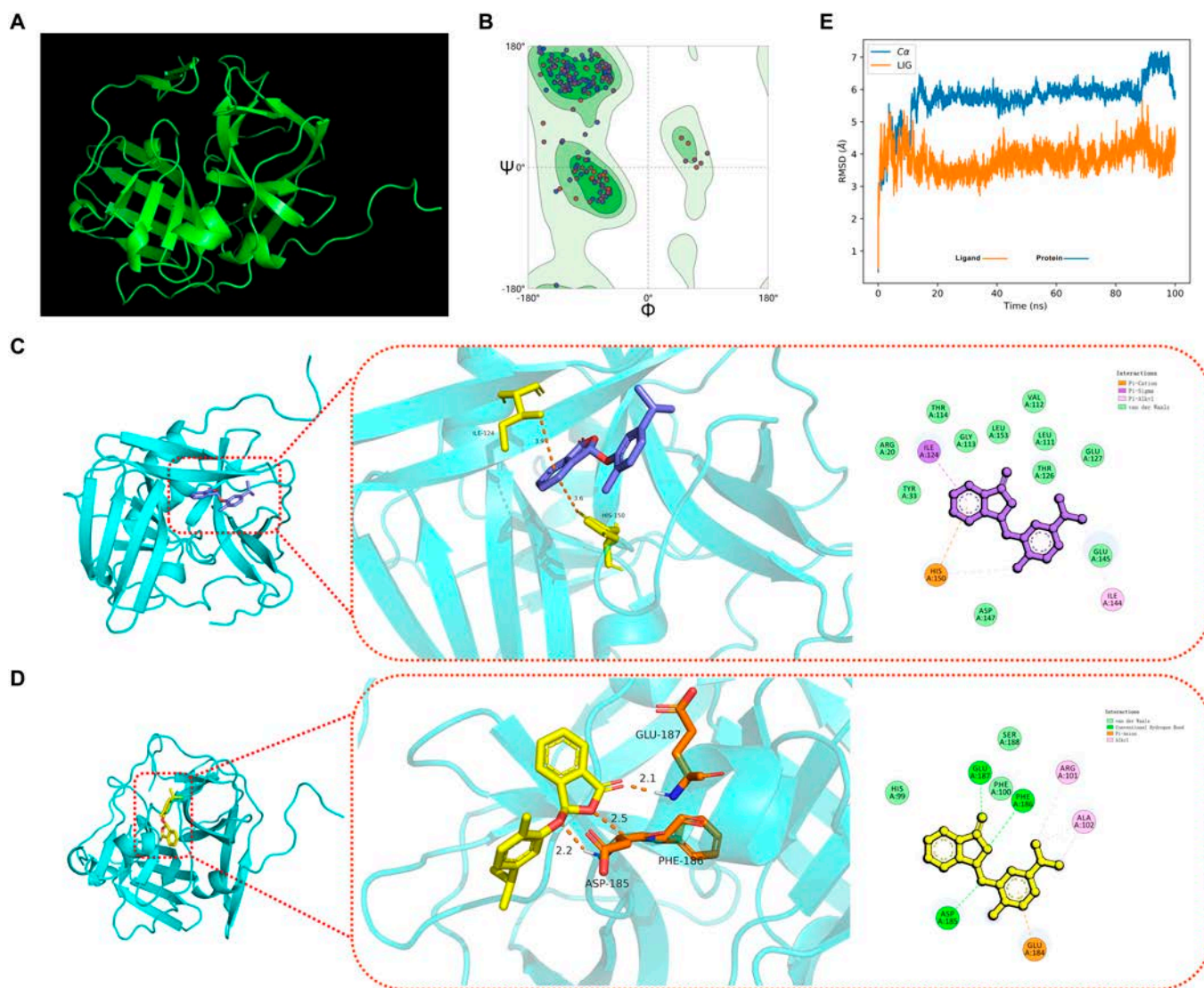


**Fig. 5.** (A) The 3-dimensional (3D) structural model of PVY Nia protein was constructed by homology modeling. (B) Homology modeling to obtain the 3D structure model of the PVY Nia protein Ramachandran plot. (C) Molecular docking of (*R*)-**3w** with the 3D structural model of PVY Nia protein. (D) Molecular docking of (*S*)-**3w** with the 3D structural model of PVY Nia protein. (E) The binding stability of compound (*R*)-**3w** to the receptor protein was evaluated by surveying the root mean square deviation values of the initial positions of the atoms via molecular dynamics simulation.

strength and quantity of H150 in binding to the drug allow it to be speculated as a key site for the following investigation.

With the H150 site in hand, our next objective was to verify its accuracy in binding to our compounds. We constructed prokaryotic expression vectors for both wild-type PVY Nia (PVY Nia<sup>WT</sup>) and mutant PVY Nia (PVY Nia<sup>H150A</sup>), and expressed and purified the corresponding proteins using *Escherichia coli*. Microscale thermophoresis (MST), a widely employed technique for studying the interaction strength between small molecules and proteins, was used to investigate the affinity of (*R*)-**3w** to Nia. The results showed that compound (*R*)-**3w** had a weak interaction with PVY CP<sup>WT</sup>, with a dissociation constant ( $K_d$ ) of 40.61  $\mu\text{M}$ , while NNM exhibited a much stronger interaction, with a  $K_d$  of 2.73  $\mu\text{M}$  (Fig. 6A), indicating that (*R*)-**3w** does not share the same molecular target as NNM. Furthermore, compound (*R*)-**3w** demonstrated a strong binding affinity to PVY Nia<sup>WT</sup>, with a  $K_d$  of 3.53  $\mu\text{M}$ . (*Rac*)-**3w** showed moderate binding affinities to both NNM and PVY Nia<sup>WT</sup>, with  $K_d$  values of 9.32 and 13.43  $\mu\text{M}$ , respectively.

Conversely, (*S*)-**3w** exhibited significantly weaker binding to PVY Nia<sup>WT</sup>, with a  $K_d$  of 26.25  $\mu\text{M}$  (Fig. 6B). After mutating histidine at position 150 to alanine, the  $K_d$  value of (*R*)-**3w** binding to the mutant PVY Nia<sup>H150A</sup> protein increased to 121.20  $\mu\text{M}$  (Fig. 6C), indicating that the binding affinity of (*R*)-**3w** with PVY Nia<sup>WT</sup> was significantly stronger than with PVY Nia<sup>H150A</sup>. These results are consistent with the previous molecular docking studies, further providing evidence for the proposal that (*R*)-**3w** targets Nia rather than CP, and that the binding ability of (*R*)-**3w** to Nia is configuration-dependent.

While *in vitro* experiments have established that H150 is a critical site for (*R*)-**3w** interaction with Nia, whether this site mediates the proliferation of PVY remains unknown. Plant viruses rely on the cellular environment of their host for effective replication. Therefore, it is necessary to further investigate the impact of H150 on PVY pathogenicity *in vivo*. To rigorously validate *in vivo* whether histidine residue H150 in the Nia protein of PVY serves as a potential binding site for compound (*R*)-**3w** and its mediated functions, this study employed a site-directed

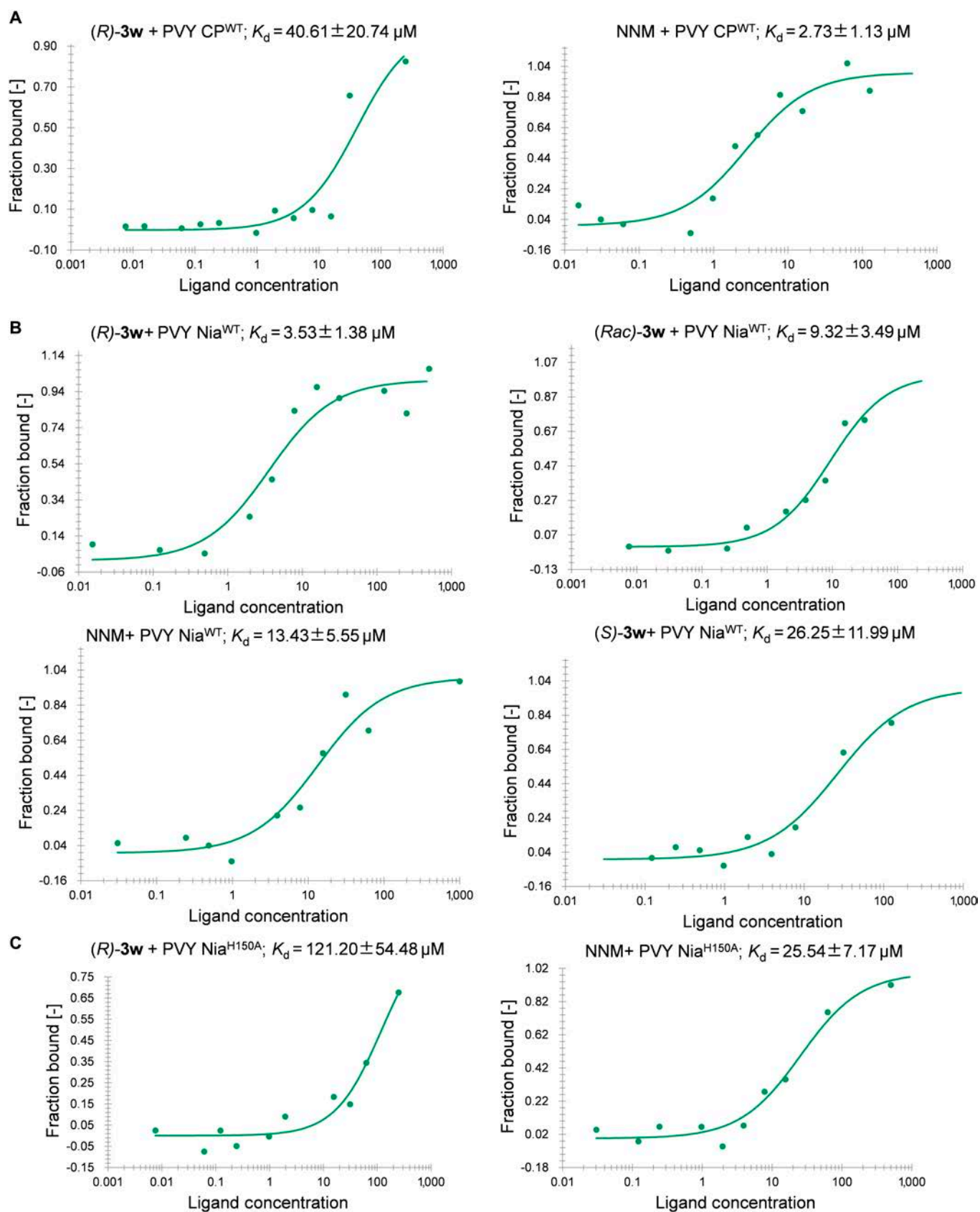


**Fig. 6.** (A) MST results of *(R)*-**3w**, NNM, and PVY CP. (B) MST results of *(R)*-**3w**, *(Rac)*-**3w**, *(S)*-**3w**, and NNM PVY Nia. (C) MST results of *(R)*-**3w**, NNM, and PVY Nia mutants.

mutagenesis strategy. Specifically, we substituted the H150 residue in the Nia protein of the pCamPVY-GFP plasmid with an alanine (Ala, A) residue [94], successfully constructing the mutant plasmid pCamPVY Nia<sup>H150A</sup>-GFP (Fig. 7A). *Agrobacterium* cultures harboring the plasmids pCamPVY-GFP and pCamPVY Nia<sup>H150A</sup>-GFP were infiltrated into *N. benthamiana* plants, respectively. Systemically infected PVY-GFP *N. benthamiana* plants exhibited typical curling and mosaic symptoms on their leaves. In contrast, plants inoculated with the mutant PVYNia<sup>H150A</sup>-GFP showed almost no apparent leaf symptoms 7 days postagroinfiltration (dpi) (as shown in the upper panel of Fig. 7B). Additionally, under ultraviolet (UV) light illumination, strong green fluorescent signals were observed in the young leaves of PVY-GFP-infected plants (as shown in the lower panel of Fig. 7B). The results from Western blot analysis, reverse transcription-polymerase chain reaction (RT-PCR), and quantitative RT-PCR (RT-qPCR) collectively demonstrate that PVY-GFP accumulates significantly in systemically infected leaves of *N. benthamiana*, whereas no accumulation of PVY is observed in the systemically infected leaves of *N. benthamiana* inoculated with PVY<sup>H150A</sup>-GFP (as shown in Fig. 7C and D). Based on these findings, we conclude that the H150 residue in the Nia protein is crucial for the systemic infection and proliferation of PVY in *N. benthamiana* plants.

PVY-Nia functions as a protease and plays a critical role in the upper stages of the viral life cycle [95]. It is involved in the cleavage of multiple polyprotein sites, and the resulting functional proteins mediate downstream pathogenic behaviors such as replication, assembly, and intercellular movement [96,97]. Additionally, reports have shown that Nia interacts with indole-3-acetic acid-amido synthetase within the host to regulate

auxin homeostasis, thereby promoting disease development [98]. Transgenic potatoes expressing scFv antibody to PVY Nia exhibit a more substantial resistance to PVY compared to those expressing scFv-antibody against PVY CP [99]. Despite its potential as an ideal target, there are fewer cases of using small molecules to abnormalize Nia function for the treatment of plant diseases. Based on the results obtained, we reasonably propose that (*R*)-**3w** binds to Nia through the H150 site, thereby affecting its ability to cleave polyproteins. This leads to a reduction in the amount or functionality of downstream proteins that mediate the formation of the VRC, ultimately disrupting the normal proliferation of the virus within the host and achieving antiviral effects (Fig. 8).

### Conclusion

To summarize, we developed an NHC-mediated functionalization reaction that promoted the synthesis of a series of phthalide ether derivatives with good conversion rates and stereoselectivity. Our catalytic protocol showed excellent functional group tolerance and scalability. Screening for bioactivity against PVY led to the discovery of a potential chiral antiviral molecule, (*R*)-**3w**. Mechanistic studies both *in vitro* and *in vivo* collectively suggested that (*R*)-**3w** impacts the capacity of Nia to cleave polyproteins by binding to the H150 residue, leading to a reduction in quantity or functionality of cut proteins. These functional proteins are vital for unlocking the subsequent formation of VRC, which enables viral proliferation. Overall, this study contributes novel candidate molecule, synthetic method, and brand-new target protein for PVY management.

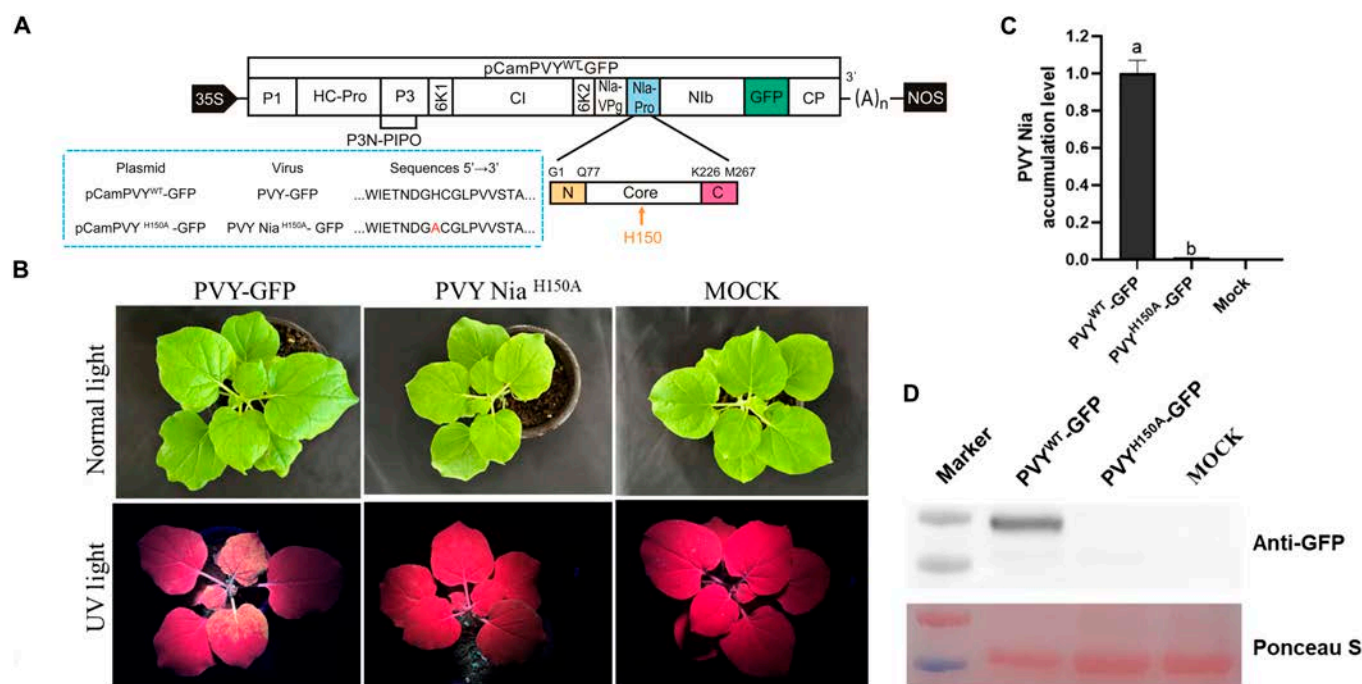


**Fig. 7.** Residue 150, where compound (*R*)-**3w** binds to PVY Nia, is critical for PVY systemic infection and self-reproduction. (A) Schematic diagram of the pCamPVY-GFP genomic structure. H150 indicated by the yellow arrow are located in the core region of PVY Nia. The site-directed mutagenized and wild-type plasmids, viruses, and sequences are displayed in the blue-lined box. (B) Symptoms (top) and green fluorescence (bottom) under UV light of *N. benthamiana* infiltrated by wild-type and mutated PVY. (C and D) The accumulation levels of PVY Nia in the systemically infected leaves of the wild-type and mutated PVY-infected *N. benthamiana* plants were analyzed at 7 days postagroinfiltration (dpi) by Western blot and quantitative RT-PCR (RT-qPCR), respectively. Staining of RuBisCO with Ponceau S was used as a sample loading control. The data are shown as means ± SD from 3 biological replicates per treatment. Different letters mean statistically significant differences ( $P < 0.05$ , one-way analysis of variance).

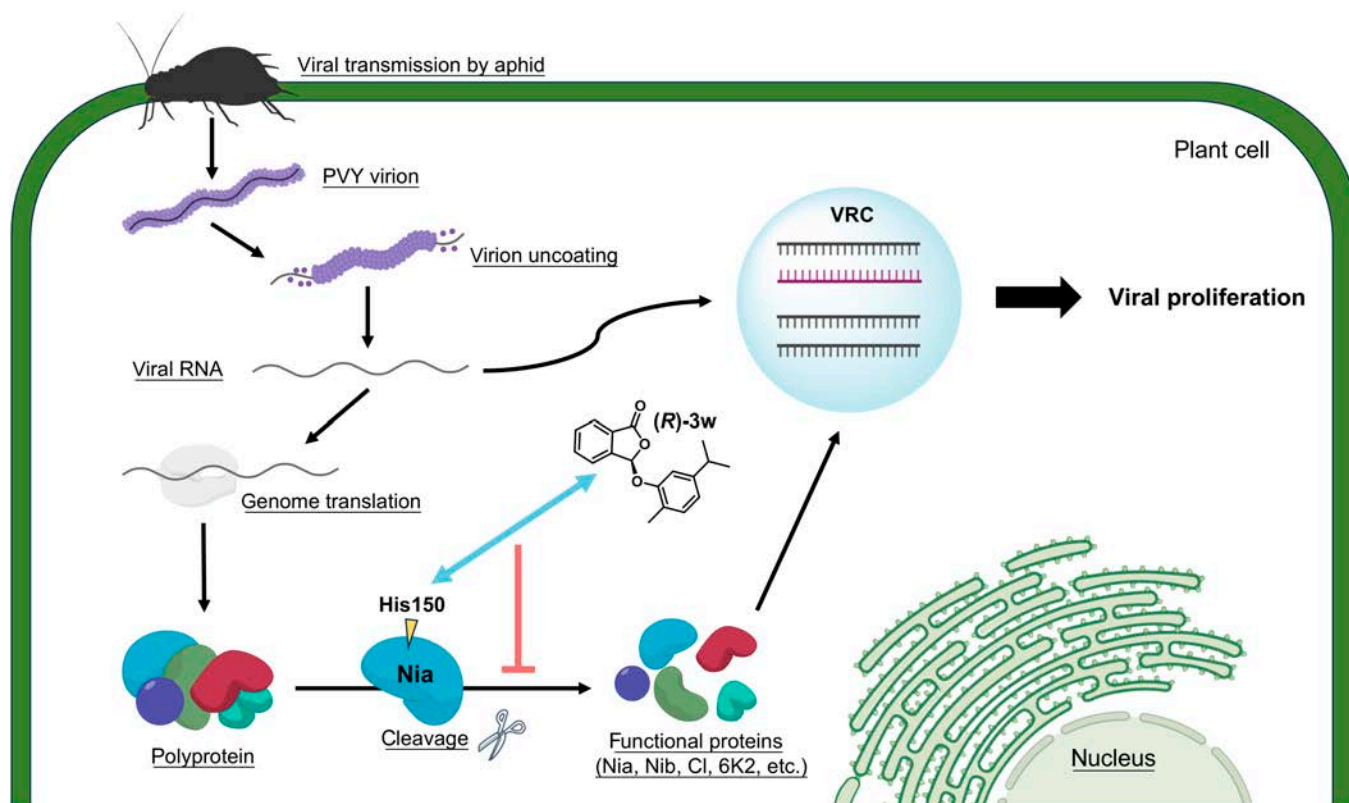


**Fig. 8.** Proposed mechanism of antiviral action of (*R*)-**3w** by combining molecular docking and a series of molecular biological verifications. (*R*)-**3w** engages in an interaction with Nia via the His150 residue. Nia holds responsibility for truncating PVY polyprotein into smaller, functional proteins. The interaction perturbs the standard cleavage mechanism, consequently leading to a marked reduction in the amount of functional proteins essential for the assembly of the VRC.

## Materials and Methods

### Chemicals and instruments

In the absence of specific notation, all reagents and solvents utilized throughout the experimental procedures were purchased from commercial sources. The chemical substances employed in this experiment, including *o*-phthalaldehyde (purity 98%; CAS: 643-79-8) and carvacrol (purity 98%; CAS: 499-75-2), were acquired from authorized commercial entities and were used without further purification. Phusion enzyme, DpnI enzyme, and DNase I enzyme were obtained from Thermo Fisher Scientific. Reverse transcriptase, Taq polymerase, and fluorescence quantitative reagent kits were purchased from Nanjing Novogene Biotechnology Co., Ltd. Trizol was obtained from Beijing Quanshijin Biotechnology Co., Ltd. Plasmid extraction kits were sourced from Omega Bio-Tek. His, glutathione S-transferase, and GFP antibodies were purchased from Wuhan Sanjing Biotechnology Co., Ltd. Enterokinase, protein markers, and DNA ladders were obtained from Shenggong Bioengineering (Shanghai) Co., Ltd.

### General synthetic method of target compounds **3a** to **3z**

To a solution of phthalaldehyde (0.12 mmol), substituted phenol (0.1 mmol), oxidant (0.12 mmol), base LiOH (0.2 mmol), and *N*-heterocarbene catalyst (0.02 mmol) in dichloromethane (2 ml), stirring was carried out overnight at room temperature. Upon completion of the reaction, the resultant mixture was initially subjected to vacuum distillation to remove the solvent,

followed by purification via column chromatography. The obtained target compounds **3a** to **3z** were structurally characterized using proton nuclear magnetic resonance ( $^1\text{H NMR}$ ),  $^{13}\text{C NMR}$ , and high-resolution mass spectrometry. Furthermore, the absolute configuration of compound **3b** was unequivocally determined as the *R* configuration through x-ray crystallographic analysis, with the crystallographic data deposited at the Cambridge Crystallographic Data Centre (CCDC) under reference number 2395277. All detailed spectroscopic data and crystallographic information are included in the Supplementary Materials.

### Antiviral activity assay against PVY

The PVY virus was inoculated into tobacco cultivar k326 and purified according to previously reported methods [100–102]. The antiviral activity of the compounds against PVY was evaluated using the classical half-leaf lesion method on appropriate host plants of the genus *Veronica* [103]. Compounds were tested at a concentration of 500  $\mu\text{g/ml}$  to assess their protective, curative, and inhibitory effects on PVY. Solutions of the compounds were prepared at concentrations of 500, 250, 125, 62.5, and 31.25  $\mu\text{g/ml}$  to evaluate the  $\text{EC}_{50}$  values of the selected compounds. Ningnanmycin and ribavirin were used as positive controls. Three plant samples were treated for each compound. Five to seven days later, the number of lesions on both sides of the leaves was counted and recorded. The inhibition rate was calculated using the formula:

Inhibition rate (%) = (Number of necrotic spots on the left side of the leaf - Number of necrotic spots on the right side

of the leaf) / Number of necrotic spots on the left side of the leaf  $\times$  100%

### Construction of an infectious wild-type clone

The wild-type plasmid pCamPVY-GFP is provided by Professors Xiangdong Li and Yanping Tian from Shandong Agricultural University [35,94]. This plasmid harbors a gene encoding GFP. Upon infection of plants such as *N. benthamiana*, it enables the expression of GFP, facilitating the visualization of gene expression through the emission of green fluorescence.

### Molecular docking

Initially, homology modeling of the PVY Nia protein was performed using SWISS-MODEL. This approach aids in predicting the 3D structure of the PVY Nia protein based on sequence similarity to known protein structures. Subsequently, the PVY Nia structure was refined using PyMOL software version 2.3.0 (Schrödinger, New York). Following this, the obtained 3D structure of the PVY Nia protein was subjected to molecular docking with the ligand (*R*)-3w. Flexible docking simulations were conducted using AutoDock 1.5.6 to elucidate the binding mode of (*R*)-3w with PVY Nia. Finally, the docking results were processed using PyMOL.

### Molecular dynamics trajectory simulations

Using the results of molecular docking as the initial conformation of the crystal, AmberTools23 was used to calculate the BCC charge of the ligand. AmberTools23 was used to build the ligand-protein complex simulation system. A box was built around the complex, with a minimum distance of 1.0 nm between the edge of the box and the protein-ligand complex. TIP3P water was added to the box, along with 3 Na<sup>+</sup> to neutralize the system's charge. The Amber 14SB force field was applied to the protein, solvent, and balancing ions, while the GAFF force field was applied to the ligand. Parmed was used to generate compatible run files for Gromacs 2023. Gromacs 2023 was used for system simulation. First, the system was energy-minimized using the steepest descent method, reaching the lowest energy in 1,205 steps. Then, 100 ps of constant-temperature equilibration and constant-pressure equilibration was performed separately. Finally, a 100-ns molecular dynamics simulation was conducted using the equilibrated results. The Gromacs trajconv module was used for preliminary processing of the simulation trajectory, including handling periodic boundary conditions and aligning the protein alpha carbon atoms to eliminate the translation and rotation of the protein-ligand complex system during the simulation. The processed trajectory was analyzed using MD analysis.

### Construction of prokaryotic expression plasmids for wild-type and mutant PVY Nia proteins

As described in Ref. [89], based on the wild-type protein gene, site-directed mutagenesis was performed to mutate the 150th amino acid residue from histidine (H150) to alanine (H150A), resulting in the PVY Nia<sup>H150A</sup> plasmid for the subsequent expression of the mutant protein (PVY Nia<sup>H150A</sup>).

### Prokaryotic expression of PVY Nia and PVY Nia<sup>H150A</sup> variants

Following the methodology outlined in Ref. [104], we have carried out the prokaryotic expression of PVY Nia and its mutant variant, PVY Nia<sup>H150A</sup>.

### MST determination of binding force

Initially, PVY Nia<sup>WT</sup> and PVY Nia<sup>H150A</sup> were labeled with fluorophores. Subsequently, the target compound and NNM were diluted to form solutions with concentration gradients. These solutions were mixed with an equal volume of protein and aspirated into capillaries for analysis. The binding fractions were plotted against the ligand concentrations, with the binding fractions serving as the ordinate and the ligand concentrations as the abscissa. By utilizing the obtained fitting data, the  $K_d$  value was derived [105,106].

### Construction of infectious mutant clone

As described in Ref. [35], site-directed mutagenesis was employed to mutate the H150 amino acid residue to A150 in the pCamPVY-GFP plasmid, based on the pCamPVY Nia<sup>WT</sup> plasmid. This process facilitated the construction of the pCamPVY Nia<sup>H150A</sup>-GFP plasmid, which was subsequently utilized for the development of subsequent *Agrobacterium* plasmids.

### Construction of the mutant PVY Nia<sup>H150A</sup>-GFP *agrobacterium* plasmid

The plasmid was built using the pCam vector as the backbone. *Agrobacterium*-mediated transformation was then employed for the introduction of the mutant PVY viral infection strains. Site-directed mutagenesis PCR strategy was used to generate the mutation, and the potential key binding sites were verified through *in vivo* assays.

### RNA extraction, RT-PCR, and RT-qPCR

Initially, *N. benthamiana* leaves were finely powdered and subjected to total RNA extraction using TransZol reagent (TransGen Biotech, Beijing, China). Following the addition of chloroform, the mixture was allowed to stand. Centrifugation was performed to collect the supernatant, which was then mixed with isopropanol for precipitation, followed by another centrifugation step. The precipitate was treated with 75% ethanol, centrifuged once again, and resuspended in diethyl pyrocarbonate-treated water to obtain the RNA. To eliminate DNA contamination, gDNA wipeout enzyme (Vazyme, Nanjing, China) was utilized. Reverse transcription was carried out using gene-specific primers or random primers along with a reverse transcriptase kit (Vazyme, Nanjing, China). PCR amplification was performed using taq DNA polymerase (Vazyme, Nanjing, China), while RT-qPCR was conducted using SYBR Green qPCR Mix (Vazyme, Nanjing, China). Detailed information regarding the primers used in this study is described in Table S2.

### Western blotting analysis

Total protein extraction from *N. benthamiana* leaves was conducted as previously described. Protein separation and identification were conducted using a 12% sodium dodecyl sulfate-polyacrylamide gel electrophoresis method. Anti-GFP antibody (Proteintech, Wuhan) was used as the primary antibody, and horseradish peroxidase-labeled goat anti-rabbit IgG (Proteintech, Wuhan) served as the secondary antibody. The target protein signals were visualized using the ChemiDoc MP Imaging System (Bio-Rad).

## Acknowledgments

We thank Prof. Xiangdong Li and Prof. Yanping Tian (Shandong Agricultural University) for their assistance with plasmid construction.

**Funding:** We acknowledge the financial support from the National Natural Science Foundation of China (nos. 32302388 and 32330087) and the Scientific Research Innovation Team of Guizhou University (no. 202403).

**Author contributions:** R.S. conceived the idea and designed the experiments. R.S., B.S., Y.R.C., and X.L. supervised the work. X.W. performed the majority of the experiments. W.Y., S.W., F.J., and Z.S. provided assistance and partial guidance for the experiments. R.S. and X.W. drafted the manuscript with the assistance of all co-authors. All authors contributed to the experiments and discussions.

**Competing interests:** The authors declare that they have no competing interests.

## Data Availability

All data are available in the manuscript or the Supplementary Materials.

## Supplementary Materials

Supplementary Text  
Fig. S1

## References

- Tyczewska A, Woźniak E, Gracz J, Kuczyński J, Twardowski T. Towards food security: Current state and future prospects of agrobiotechnology. *Trends Biotechnol.* 2018;36(12):1218–1229.
- Cole M, Augustin M, Robertson MJ, Manners JM. The science of food security. *NPJ Sci Food.* 2018;2:14.
- Shelley M. FAO, IFAD, and WFP. The state of food insecurity in the world 2015: Meeting the 2015 International Hunger Targets: Taking stock of uneven Progress. Rome: FAO, 2015. *Adv Nutr.* 2015;6:623–624.
- Paterson S, Gómez-Cortés P, Fuente M, Hernández-Ledesma B. Bioactivity and digestibility of microalgae *Tetraselmis* sp. and *Nannochloropsis* sp. as basis of their potential as novel functional foods. *Nutrients.* 2023;15(2):477.
- Pretty J. Intensification for redesigned and sustainable agricultural systems. *Science.* 2018;362(6417):eaav0294.
- Anderson W, Seager R, Baethgen W, Cane M, You L. Synchronous crop failures and climate-forced production variability. *Sci Adv.* 2019;5(7):eaaw1976.
- Carvajal-Yepes M, Cardwell K, Nelson A, Garrett K, Giovani B, Saunders D, Kamoun S, Legg JP, Verdier V, Lessel J, et al. A global surveillance system for crop diseases. *Food Secur.* 2019;364(6447):1237–1239.
- Jackson P, Kennedy K. The global strategy for plant conservation: A challenge and opportunity for the international community. *Trends Plant Sci.* 2009;14(11):578–580.
- Daum R. The plant protection discipline problems and possible developmental strategies. *Bull Entomol Soc Am.* 1979;25(4):290–291.
- Komarnytsky S, Retchin S, Vong CI, Lila MA. Gains and losses of agricultural food production: Implications for the twenty-first century. *Annu Rev Food Sci Technol.* 2022;13(1):239–261.
- Ataei P, Gholamrezai S, Movahedi R, Aliabadi V. An analysis of farmers' intention to use green pesticides: The application of the extended theory of planned behavior and health belief model. *J Rural Stud.* 2021;81:374–384.
- Bruce S, Guy P, Rezzi S, Rossl A. Quantitative measurement of betaine and free choline in plasma, cereals and cereal products by isotope dilution LC-MS/MS. *J Agric Food Chem.* 2010;58(4):2055–2061.
- Gao M, Meng J, Lv H, Zhang X. Highly regio- and enantioselective Synthesis of  $\gamma$ ,  $\delta$ -unsaturated amido esters by catalytic hydrogenation of conjugated enamides. *Angew Chem Int Ed Engl.* 2015;54(6):1885–1887.
- Zhu G-L, Zhang X-D, Yang L-J, Xie J-H, Che D-Q, Zhou Q-L, Yan P-C, Li Y-Q. Ir/SpiroPAP catalyzed asymmetric hydrogenation of a key intermediate of Montelukast: Process development and potential impurities study. *Org Process Res Dev.* 2016;20(1):81–85.
- List B. Introduction: Organocatalysis. *Chem Rev.* 2007;107(12):5413–5415.
- MacMillan DW. The advent and development of organocatalysis. *Nature.* 2008;455(7211):304–308.
- Ahrendt K, Borths C, MacMillan DW. New strategies for organic catalysis: The first highly enantioselective organocatalytic Diels-Alder reaction. *J Am Chem Soc.* 2000;122(17):4243–4244.
- Dolling UH, Davis P, Grabowski EJ. Efficient catalytic asymmetric alkylations. 1. Enantioselective synthesis of (+)-indacrinone via chiral phase-transfer catalysis. *J Am Chem Soc.* 1984;106(2):446–447.
- Hughes DL, Dolling UH, Ryan KM, Schoenewaldt EF, Grabowski EJ. Efficient catalytic asymmetric alkylations. 3. A kinetic and mechanistic study of the enantioselective phase-transfer methylation of 6,7-dichloro-5-methoxy-2-phenyl-1-indanone. *J Org Chem.* 1987;52(21):4745–4752.
- Xu F, Zacuto M, Yoshikawa N, Desmond R, Hoerrner S, Itoh T, Journet M, Humphrey GR, Cowden C, Strotman N, et al. Asymmetric synthesis of telcagepant, a CGRP receptor antagonist for the treatment of migraine. *J Org Chem.* 2010;75(22):7829–7841.
- Kiesewetter MK, Shin EJ, Hedrick JL, Waymouth RM. Organocatalysis: Opportunities and challenges for polymer synthesis. *Macromolecules.* 2010;43(5):2093–2107.
- Zhang X, Fevre M, Jones G, Waymouth RM. Catalysis as an enabling science for sustainable polymers. *Chem Rev.* 2017;118(2):839–885.
- Smh K. Composite nature of certain potato viruses of the mosaic group. *Nature.* 1931;127(3210):702.
- Aramburu J, Galipienso L, Matas M. Characterization of potato virus Y isolates from tomato crops in Northeast Spain. *Eur J Plant Pathol.* 2006;115:247–258.
- Yang X, Li Y, Wang A. Research advances in potyviruses: From the laboratory bench to the field. *Annu Rev Phytopathol.* 2021;59:1–29.
- Godfray HC, Beddington JR, Crute IR, Haddad L, Lawrence D, Muir JF, Pretty J, Robinson S, Thomas SM, Toulmin C. Food security: The challenge of feeding 9 billion people. *Science.* 2010;327(5967):812–818.
- Deja-Sikora E, Mercy L, Baum C, Hryniewicz K. The contribution of Endomycorrhiza to the performance of

- potato virus Y*-infected solanaceous plants: Disease alleviation or exacerbation? *Front Microbiol.* 2019;10:516.
28. Eastop V, Banks C. Suspected insecticide resistance mechanism in the peach-potato aphid. *Nature.* 1970;225(5236):970–971.
  29. Guo Y, Zhang Y, Dong F, Wu X, Pan X, Zheng Y, Xu J. Pesticide thiamethoxam in seed treatment: Uptake, metabolic transformation and associated synergistic effects against wheat aphids. *Sci Total Environ.* 2024;949:Article 174955.
  30. Ullah R, Gao F, Sikandar A, Wu H. Insights into the effects of insecticides on aphids (Hemiptera: Aphididae): Resistance mechanisms and molecular basis. *Int J Mol Sci.* 2023;24(7):6750.
  31. Urcuqui-Inchima S, Haenni A, Bernardi F. Potyvirus proteins: A wealth of functions. *Virus Res.* 2001;74(1-2):157–175.
  32. Ba L, Wei C, Zhang J, Song R. Design, synthesis, and anti-PVY biological activity of 1,3,5-triazine derivatives containing piperazine structure. *Int J Mol Sci.* 2023;24(9):8280.
  33. Wu Z, Huang M, Jiang J, Zhang C, Hao G, Chen M, Li QX, Jia M, Liu J, Li X. Ningnanmycin activates defense systems against potato virus Y in *Nicotiana benthamiana*. *J Agric Food Chem.* 2024;72(48):26633–26643.
  34. Cui H, Wu Z, Zhang L, Wu D, Hu D, Zhang J. Discovery of pyrido[1,2- $\alpha$ ] pyrimidinone mesoionic compounds as potential control agents against potato virus Y. *J Agric Food Chem.* 2024;72(23):12925–12934.
  35. Wei C, Zhao C, Li J, Li C, Song B, Song R. Innovative arylimidazole-fused phytovirucides via carbene-catalyzed [3+4] cycloaddition: Locking viral cell-to-cell movement by out-competing virus capsid-host interactions. *Adv Sci.* 2024;11(19):2309343.
  36. Li X, Hao G, Wang Q, Chen Z, Ding Y, Yu L, Hu D, Song B. Ningnanmycin inhibits tobacco mosaic virus virulence by binding directly to its coat protein discs. *Oncotarget.* 2017;8(47):82446–82458.
  37. Derkacz D, Bernat P, Krasowska A. K143R amino acid substitution in 14- $\alpha$ -demethylase (Erg11p) changes plasma membrane and cell wall structure of *Candida albicans*. *Int J Mol Sci.* 2022;23(3):1631.
  38. Otum CC, Rivière E, Barnard M, Loubser J, Williams MJ, Streicher EM, van Rie A, Warren RM, Klopper M. Site-directed mutagenesis of *mycobacterium tuberculosis* and functional validation to investigate potential bedaquiline resistance-causing mutations. *Sci Rep.* 2023;13(1):9212.
  39. Almási A, Nemes K, Csömör Z, Tóbiás I, Palkovics L, Salánk K. A single point mutation in tomato spotted wilt virus NSs protein is sufficient to overcome Tsw-gene-mediated resistance in pepper. *J Gen Virol.* 2017;98(6):1521–1525.
  40. Luo Z, Deng Y, Luo B, Li Y, Lan Q, Fan J, Xue W, Tang L, Fan L. Design and synthesis of novel n-butylphthalide derivatives as promising botanical fungicides. *Naturforsch.* 2021;76(3-4):117–127.
  41. Li Y, Luo Z, Zhou A, Liu W, Fan J, Miao J, Guo B, Tang L, Fan L. Design and synthesis of novel benzoxazole/chromene-phthalide scaffolds hybrids as potential natural products-based fungicide. *Nat Prod Res.* 2024;38(14):2441–2446.
  42. Guo Z, Zhou P, Song H, Liu Y, Zhang J, Li Y, Wang Q. Design, synthesis, and bioactivities of phthalide and coumarin derivatives based on the biosynthesis and structure simplification of gossypol. *J Agric Food Chem.* 2021;69(50):15123–15135.
  43. Jia Y, Shao C, Wang C, Ma J, Guan F. Pestalotioid a, a new antiviral phthalide derivative from a soft coral-derived fungus *Pestalotiopsis* sp. *Nat Prod Sci.* 2015;21(4):227–230.
  44. Liu Y, Liu S, Luo X, Wu X, Ren J, Huang X, Feng S, Lin X, Ren M, Dong P. Antifungal activity and mechanism of thymol against *Fusarium oxysporum*, a pathogen of potato dry rot, and its potential application. *Postharvest Biol Technol.* 2022;192:Article 112025.
  45. Cutillas A, Carrasco A, Martinez-Gutierrez R, Tomas V, Tudela J. Thyme essential oils from Spain: Aromatic profile ascertained by GC-MS, and their antioxidant, anti-lipoxygenase and antimicrobial activities. *J Food Drug Anal.* 2018;26(2):529–544.
  46. Saoulajan C, Boujida N, Mihyaoui AE, Baakili AE, Alshahrani MM, Lee L-H, Bouyahya A. Phytochemistry, pharmacological investigations, industrial applications, and encapsulation of *Thymbra capitata* L. a review. *Trends Food Sci Technol.* 2022;129:463–491.
  47. Lou M, Li S, Jin F, Yang T, Song R, Song B. Pesticide engineering from natural vanillin: Recent advances and a perspective. *Engineering.* 2024;43:241–257.
  48. Ming H, Struble J, Bode J. Highly enantioselective azadiene Diels-Alder reactions catalyzed by chiral N-heterocyclic carbenes. *J Am Chem Soc.* 2006;37(46):8418–8420.
  49. Kerr M, Read de Alaniz J, Rovis T. A highly enantioselective catalytic intramolecular Stetter reaction. *J Am Chem Soc.* 2002;34(35):10298–10299.
  50. Yao H, Zhou Y, Chen X, Zhang P, Xu J, Liu H. N-heterocyclic carbene catalytic [4 + 2] cyclization of 3-alkylenyloxindoles with enals:  $\gamma$ -carbon activation for enantioselective assembly of spirocarbocyclic oxindoles. *J Org Chem.* 2016;81(19):8888–8899.
  51. Huynh HV, Lam TT, Luong HTT. Anion influences on reactivity and NMR spectroscopic features of NHC precursors. *RSC Adv.* 2018;8(61):34960–34966.
  52. Sohn S, Bod J. N-heterocyclic carbene catalyzed C-C bond cleavage in redox esterifications of chiral formylcyclopropanes. *Angew Chem Int Ed Engl.* 2006;45(36):6021–6024.
  53. Mahatthananchai J, Bode J. The effect of the N-mesityl group in NHC-catalyzed reactions. *Chem Sci.* 2012;3(1):192–197.
  54. Alaniz J, Kerr M, Moore L, Rovis T. ChemInform abstract: Scope of the asymmetric intramolecular Stetter reaction catalyzed by chiral nucleophilic triazolinylidene carbenes. *J Org Chem.* 2008;73(6):2033–2040.
  55. Buravlev E, Shevchenko O. Bisphenols analogues derived from natural phenols: Synthesis and evaluation of antioxidant capacity. *Chem Pap.* 2023;77:6169–6182.
  56. Kachur K, Suntres Z. The antibacterial properties of phenolic isomers, carvacrol and thymo. *Crit Rev Food Sci Nutr.* 2020;60(18):3042–3053.
  57. Paduch-Cichal E, Mirzwa-Mróz E, Wojciechowska P, Bączek K, Kosakowska O, Węglarz Z, Szyndel MS. Antiviral activity of selected essential oils against cucumber mosaic virus. *Plants.* 2023;12(1):18.
  58. Wang X, Gong C, Zhao Y, Shen L. Transcriptome and resistance-related genes analysis of *Botrytis cinerea* B05. 10 strain to different selective pressures of cyprodinil and fenhexamid. *Front Microbiol.* 2018;9:2591.
  59. Liu Y, Chen Q, Mou C, Pan L, Duan X, Chen X, Chen H, Zhao Y, Lu Y, Jin Z, et al. Catalytic asymmetric acetalization

- of carboxylic acids for access to chiral phthalidyl ester prodrugs. *Nat Commun.* 2019;10:Article 1675.
60. Liu Y, Zhong Z, Tang Y, Wang H, Vummaleti SVC, Peng X, Peng P, Zhang X, Chi YR. Carbene-catalyzed chirality-controlled site-selective acylation of saccharides. *Nat Commun.* 2025;16(1):54.
  61. Lv WX, Chen H, Zhang X, Ho CC, Liu Y, Wu S, Wang H, Jin Z, Chi YR. Programmable selective acylation of saccharides mediated by carbene and boronic acid. *Chem.* 2022;8(5):1518–1534.
  62. Liu Y, Majhi PK, Song R, Mou C, Hao L, Chai H, Jin Z, Chi YR. Carbene-catalyzed dynamic kinetic resolution and asymmetric acylation of hydroxyphthalides and related natural products. *Angew Chem Int Ed Engl.* 2020;59(10):3887–3891.
  63. Samanta R, de Sarkar S, Roland F, Grimme S, Studer A. N-heterocyclic carbene (NHC) catalyzed chemoselective acylation of alcohols in the presence of amines with various acylating reagents. *Chem Sci.* 2013;4(5):2177–2184.
  64. Cai Y, Lv Y, Shu L, Jin Z, Chi Y, Ting L. Access to axially chiral aryl aldehydes via carbene-catalyzed nitrile formation and desymmetrization reaction. *Research.* 2024;7, 0293.
  65. Rouh H, Tang Y, Xu T, Yuan Q, Zhang S, Wang J, Jin S, Wang Y, Pan J, Wood HL, et al. Aggregation-induced synthesis (AIS): Asymmetric synthesis via chiral aggregates. *Research.* 2022;2022:9865108.
  66. Rahman A, Wang Y, Xu T, Reddy K, Jin S, Yan J, Yuan Q, Unruh D, Liang R, Li G. Discovery of staircase chirality through the design of unnatural amino acid derivatives. *Research.* 2024;7:0550.
  67. Xu T, Wang Y, Jin S, Rahman A, Yan X, Yuan Q, Liu H, Wang JY, Yan W, Jiao Y, et al. Amino turbo chirality and its asymmetric control. *Research.* 2024;7:0474.
  68. Tang Y, Wang Y, Yuan Q, Zhang S, Wang J, Jin S, Xu T, Pan J, Surowiec K, Li G. Aggregation-induced catalysis: Asymmetric catalysis with chiral aggregates. *Research.* 2023;6:0163.
  69. Liu J, Zheng Y, Dong F, Li Y, Wu X, Pan X, Zhang Y, Xu J. Insight into the long-lasting control efficacy of neonicotinoid imidacloprid against wheat aphids during the entire growth period. *J Agric Food Chem.* 2023;71(32):12167–12176.
  70. Guo P, An X, Pan X, Xu J, Wu X, Zheng Y, Dong F. Rational understanding of chiral fungicide penthiopyrad stereoselectivity: Bioactivity, aquatic toxicity and cytotoxicity. *Sci Total Environ.* 2023;905:Article 166969.
  71. Zhang P, Yang F, Ran L, Yang C, Tang C, Ke X, Chen J, Xiao W, He L, Xu Z. Systemic evaluation of novel acaricide hexythiazox for bioactivity improvement and risk reduction at the enantiomer level. *Sci Total Environ.* 2024;926: Article 171907.
  72. Ito T, Handa A. Teratogenic effects of thalidomide: Molecular mechanisms. *Cell Mol Life Sci.* 2011;68(9):1569–1579.
  73. Yamamoto J, Ito T, Yamaguchi Y, Handa H. Discovery of CRBN as a target of thalidomide: A breakthrough for progress in the development of protein degraders. *Chem Soc Rev.* 2022;51(15):6234–6250.
  74. Qiu D, Dong Y, Zhang Y, Li S, Shi F. Plant immunity inducer development and application. *Mol Plant-Microbe Interact.* 2017;5(5):355–360.
  75. Gao Q, Kachroo A, Kachroo P. Chemical inducers of systemic immunity in plants. *J Exp Bot.* 2014;65(7):1849–1855.
  76. Linthorst JHM, Van Loon LC. Pathogenesis-related proteins of plants. *Crit Rev Plant Sci.* 1991;10(2):123–150.
  77. Gan X, Zhang W, Lan S, Hu D. Novel cyclized derivatives of ferulic acid as potential antiviral agents through activation of photosynthesis. *J Agric Food Chem.* 2023;71(3):1360–1380.
  78. Nagy P, Pogany J. The dependence of viral RNA replication on co-opted host factors. *Nat Rev Microbiol.* 2012;10(2): 137–149.
  79. Liu H, Zhao X, Yu M, Meng L, Zhou T, Shan Y, Liu X, Xia Z, An M, Wu Y. Transcriptomic and functional analyses indicate novel anti-viral mode of actions on tobacco mosaic virus of a microbial natural product  $\epsilon$ -poly-l-lysine. *J Agric Food Chem.* 2021;69(7):2076–2086.
  80. Jeyaraj G, Alphonse V, Jayanthi P, Angelin N, Geetanjali S, Govindan G. Harnessing the potential of CRISPR/Cas system for enhancing virus resistance in plants: Targets, strategies, and challenges. *Physiol Mol Plant Pathol.* 2024;129:102202.
  81. Rizk M, Ketta H, Shabana Y. Discovery of novel *Trichoderma*-based bioactive compounds for controlling potato virus Y based on molecular docking and molecular dynamics simulation techniques. *Chem Biol Technol Agric.* 2024;11(1):110.
  82. Deng Y, Cai H, Jin J, Song C, Lv X, Jin Z, Chi YR. Synthesis of planar chiral compounds containing  $\alpha$ -amino phosphonates for Antiplant virus applications against potato virus Y. *J Agric Food Chem.* 2024;72(21):11917–11927.
  83. Shu J, Cao K, Fei C, Dai H, Li Y, Cao Y, Zhou T, Yu M, Xia Z, An M, et al. Antiviral mechanisms of anisomycin produced by *Streptomyces albulus* SN40 on potato virus Y. *J Agric Food Chem.* 2024;72(7):3506–3519.
  84. Yang X, Liu D, Wei C, Li J, Zhao C, Tian Y, Li X, Song B, Song R. Rational design of 2H-chromene-based antiphytovirals that inhibit virion assembly by outcompeting virus capsid-RNA interactions. *iScience.* 2024;27(11): Article 111210.
  85. May J. Plant viruses and biomolecular condensates: Novel perspectives in virus replication strategies. *New Phytol.* 2024;243(5):1636–1638.
  86. Jia Z, Rui P, Fang X, Han K, Yu T, Lu Y, Zheng H, Chen J, Yan F, Wu G. Proteolysis of host DEAD-box RNA helicase by potyviral proteases activates plant immunity. *New Phytol.* 2025;245(4):1655–1672.
  87. Yuan W, Chen X, Du K, Jiang T, Li M, Cao Y, Li X, Doehlemann G, Fan Z, Zhou T. N1a-Pro of sugarcane mosaic virus targets corn cysteine protease 1 (CCP1) to undermine salicylic acid-mediated defense in maize. *PLOS Pathog.* 2024;20(3):e1012086.
  88. Lin H, Chen X, Chen J, Wang D, Wu F, Lin S, Zhan CG, Wu JW, Yang WC, Yang GF. Crystal structure of 4-hydroxyphenylpyruvate dioxygenase in complex with substrate reveals a new starting point for herbicide discovery. *Research.* 2019;2019:2602414.
  89. Kežar A, Kavčič L, Polák M, Nováček J, Gutiérrez-Aguirre I, Žnidarič M, Coll A, Stare K, Gruden K, Ravnikar M, et al. Structural basis for the multitasking nature of the potato virus Y coat protein. *Sci Adv.* 2019;5(7):eaaw3808.
  90. Oliveira L, Volpon L, Rahardjo A, Osborne M, Culjkovic-Kraljacic B, Trahan C, Oeffinger M, Kwok B, Borden K. Structural studies of the eIF4E–VPg complex reveal a direct competition for capped RNA: Implications for translation. *PNAS.* 2019;116:201904752.
  91. Kitchen D, Decornez H, Furr J, Bajorath J. Docking and scoring in virtual screening for drug discovery: Methods and applications. *Nat Rev Drug Discov.* 2004;3(11):935–949.

92. Storer M, Hunter C. The surface site interaction point approach to non-covalent interactions. *Chem Soc Rev*. 2022;51(24):10064–10082.
93. Yu Y, Saleh A, Sun X, Wang Z, Lu Y, Zhang D, Zhang C. Exploring the interaction between myofibrillar proteins and pyrazine compounds: Based on molecular docking, molecular dynamics simulation, and multi-spectroscopy techniques. *Int J Biol Macromol*. 2023;253(Pt 2):Article 126844.
94. Cheng DJ, Tian YP, Geng C, Guo Y, Jia MA, Li XD. Development and application of a full-length infectious clone of potato virus Y isolate belonging to SYR-I strain. *Virus Res*. 2020;276:Article 197827.
95. Sanfaçon H. 3C-like proteases at the interface of plant-virus-vector interactions: Focus on potyvirus NIa proteases and secovirus proteases. *Virology*. 2025;602: Article 110299.
96. Li F, Leier A, Liu Q, Wang Y, Xiang D, Akutsu T, Webb GI, Smith AI, Marquez-Lago T, Li J, et al. Procleave: Predicting protease-specific substrate cleavage sites by combining sequence and structural information. *Genomics Proteomics Bioinformatics*. 2020;18(1):52–64.
97. Chen M, Shang Y, Cui W, Wang X, Zhu J, Dong H, Wang H, Su T, Wang W, Zhang K, et al. Molecular mechanism of proteolytic cleavage-dependent activation of CadC-mediated response to acid in *E. coli*. *Commun Biol*. 2024;7(1):1335.
98. Gnanasekaran P, Zhai Y, Kamal H, Smertenko A, Pappu H. A plant virus protein, NIa-pro, interacts with indole-3-acetic acid-amido synthetase, whose levels positively correlate with disease severity. *Front Plant Sci*. 2023;14:1112821.
99. Gargouri-Bouzid R, Jaoua L, Rouis S, Saïdi M, Bouaziz D, Ellouz R. PVY-resistant transgenic potato plants expressing an anti-Nia protein scFv antibody. *Mol Biotechnol*. 2006;33(2):133–140.
100. Iannelli D, D'Apice L, Cottone C, Viscardi M, Scala F, Zoina A, Del Sorbo G, Spigno P, Capparelli R. Simultaneous detection of cucumber mosaic virus, tomato mosaic virus and potato virus Y by flow cytometry. *J Virol Methods*. 1997;69(1-2): 137–145.
101. He F, Shi J, Wang Y, Wang S, Chen J, Gan X, Song B, Hu D. Antiviral activity, and mechanisms of purine nucleoside derivatives containing a sulfonamide moiety. *J Agric Food Chem*. 2019;67(31):8459–8467.
102. Chen J, Shi J, Yu L, Liu D, Gan X, Song B, Hu D. Design, synthesis, antiviral bioactivity, and defense mechanisms of novel dithioacetal derivatives bearing a strobilurin moiety. *J Agric Food Chem*. 2018;66(21):5335–5345.
103. Wei C, Zhang J, Shi J, Gan X, Hu D, Song B. Synthesis. Antiviral activity, and induction of plant resistance of indole analogues bearing dithioacetal moiety. *J Agric Food Chem*. 2019;67(50):13882–13891.
104. Rabie M, Aleem E, Elwan E, Fattouh F. Potato virus Y recombinant coat protein production in *Escherichia coli*: Applications in antibody production and virus detection. *J Phytopathol*. 2021;169(7-8):409–418.
105. Ran L, Ding Y, Luo L, Gan X, Li X, Chen Y, Hu D, Song B. Interaction research on an antiviral molecule that targets the coat protein of southern rice black-streaked dwarf virus. *Int J Biol Macromol*. 2017;103:919–930.
106. Wang Z, Li X, Wang W, Zhang W, Yu L, Hu D, Song B. Interaction research on the antiviral molecule dufulin targeting on southern rice black streaked dwarf virus p9-1 nonstructural protein. *Viruses*. 2015;7(3):1454–1473.